ELECTRONIC SEISMOLOGIST

Interactive Visualization of Spatially Amplified GNSS Time-Series Position Fields

by Brendan J. Meade, William T. Freeman, James Wilson, Fernanda Viegas, and Martin Wattenberg

ABSTRACT

Global Navigation Satellite System (GNSS) position time series are used pervasively in earthquake science to measure the surface response to earthquake cycle deformation. Characteristic usage cases are focused on the temporal windowing of position data to isolate coseismic, postseismic, or interseismic deformation. Here, we present an interactive visualization approach for the temporal evolution of GNSS time session in 2D in which the position estimates are amplified relative to their true positions, or are amplified relative to a reference state. This approach enables a rapid visual assessment of deformation patterns across all phases of the earthquake cycle in relation to topographic structure and active faults including azimuth reversal of coseismic and interseismic deformation.

INTRODUCTION

Over the last two decades, Global Navigation Satellite System (GNSS) position time-series measurements have emerged as an integral part of earthquake science, enabling the imaging of coseismic slip distributions (e.g., Shen *et al.*, 1996; Simons *et al.*, 2011), quantification of slip deficit rates, and the discovery of silent earthquakes (e.g., Dragert *et al.*, 2001; Graham *et al.*, 2014). Classical approaches to visualize these data have fallen into two general categories: (1) map view of velocity/displacement vectors over a fixed time interval and (2) time versus position plots of GNSS component (east, north, and up) time series. Each of these approaches has proved to be informative ways of understanding the spatial distribution crustal movements and the time evolution of solid-earth deformation.

Maps with arrow representations of GNSS velocities/displacements are used to visualize and understand both tectonic and earthquake cycle activity (e.g., Feigl *et al.*, 1990, 1993; Hager *et al.*, 1991; Sella *et al.*, 2002; Sagiya, 2004; Kreemer *et al.*, 2014; see Data and Resources). The velocities and displacements are derived from differential position measurements and represent snapshots of activity within a finite time interval (Fig. 1). With the recent rise of very dense GNSS data sets in Japan (Sagiya, 2004) and the western United States (see Data and Resources), it has become more challenging to use static arrow plots to meaningfully visualize all GNSS data in a given region (Fig. 1), as the velocity arrows plot over one another without using multiple velocity scales on a single figure (Wang *et al.*, 2011). Time-dependent arrow animations of GNSS displacements following the 2011 M_w 9 Tohoku-Oki earthquake have revealed the spatially coherent propagation of both body and surface waves (Grapenthin and Freymueller, 2011, see Data and Resources). Time-dependent vertical velocity changes have also been visualized as animated scatter plots (see Data and Resources).

More typically, time-dependent GNSS time series are visualized as individual displacement components (east, north, and up) as a function of time (e.g., Savage and Svarc, 1997; Dragert *et al.*, 2001, Ergintav *et al.*, 2009; Mavrommatis *et al.*, 2014; Loveless and Meade, 2016). This enables the identification of the temporal relationships and relative magnitudes of deformation between different phases of the earthquake cycle (Fig. 2). Interseismic deformation appears relatively steady in time with semiharmonic annual perturbations at rates of < 100 mm/yr. Coseismic deformation is readily identified as jumps in daily (or subdaily) position estimates and postseismic appears as nonlinear variations in position estimates over the years to decades following large earthquakes. Additionally, slow or silent earthquakes may appear as motion reversals in interseismic velocity trends (e.g., Dragert *et al.*, 2001) or as time-dependent changes in the slope of interseismic velocity components (e.g., Nishimura *et al.*, 2004; Meade and Loveless, 2009; Mavrommatis *et al.*, 2014). Web-based browsing of GNSS time series is available at numerous archival and data distribution sites (see Data and Resources) and the MATLAB-based TSView tool (see Data and Resources, Herring, 2003) enables the interactive removal jumps and trends from locally hosted time-series data are to isolate individual stages of the earthquake cycle.

 doi: 10.1785/0220160169

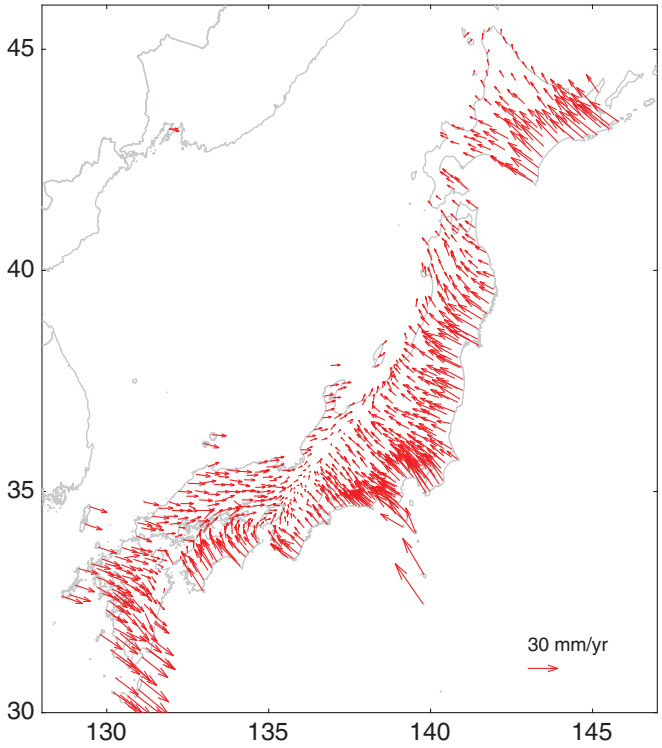

▲ **Figure 1.** Global Navigation Satellite System (GNSS) velocity vectors in Japan from 1997 to 2001 in a nominal Eurasian reference frame (Loveless and Meade, 2010). Velocities in Honshu and Hokkaido are closest to the Pacific plate and driven toward the northwest due to interseismic coupling of the Japan subduction zone and decay quickly with distance toward the Sea of Japan. The details of the GNSS velocity distribution in the Tokai region are difficult to discern with this presentation style due to the relatively high density of GNSS stations in this region.

A recent innovation in the visualization of GNSS position time series was the development of geodograms (Wernicke and Davis, 2010). Designed to illuminate low magnitude, spatially coherent behavior plots show positive and negative trends after a linear trend has been subtracted from GNSS position time series projecting along an azimuth. These visualizations have been used to understand nonlinear interseismic deformation trends and led to the inference of in the Basin and Range Province and led to the hypothesis inference of the occurrence of intracontinental slow-slip events (Wernicke and Davis, 2010).

INTERACTIVE VISUALIZATION OF GNSS-AMPLIFIED POSITION TIME SERIES IN SPACE

An alternative to segregating map view temporal snapshots and time-series approach is to visualize GNSS position time series directly on a map. Here, the approach is straightforward: simply magnify the daily longitude and latitude position changes to show tracks of the position time-series evolution at each GNSS station. These magnified horizontal position time-series tracks can be shown as trails on top of shaded relief topography

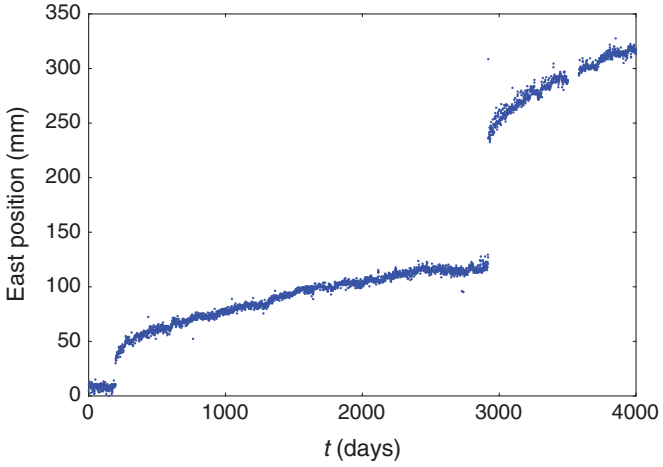

▲ **Figure 2.** Example ~11-year GNSS time series from east component of GEONET GNSS 020893 in Japan. The large upward jumps in the time series represent the coseismic displacements from large earthquakes. The nonlinear curvature following the two coseismic jumps indicates rapid postseismic deformation.

to provide a sense of position evolution in geographic context. Static renderings of this sort suffer from the same problem that static GNSS velocity vector images do; in regions of high spatial density of GNSS, station tracks overlap significantly with one another, obscuring details so that previous track visualization work has focused on small spatial scales (Barbot *et al.*, 2012) or without geographic context (Radiguet *et al.*, 2011). Instead of trying to solve this problem with static images, we take the approach of enabling dynamic interaction with the GNSS position time-series tracks. To address this challenge, we developed a JavaScript-based viewer for GNSS position time-series tracks, which enables interactive zooming and rescaling in real time.

The central idea is to take the initial GNSS coordinates of each station and draw lines connecting their daily position estimates, in which the change in daily longitude and latitude is amplified by a factor of α. The first coordinate of each track is the initial longitude and latitude position of each GNSS time series t_0. A first-order approximation of the amplified longitude and latitude track positions is given by $\phi_p(t) = \phi(t_0) + \alpha(\phi(t) - \phi(t_0))$ and $\lambda_p(t) = \lambda(t_0) + \alpha(\lambda(t) - \lambda(t_0))$, in which $\phi(t)$ and $\lambda(t)$ give the longitude and latitude of a GNSS station at time t. The amplified station longitudes and latitudes, relative to initial coordinates $\phi(t_0)$ and $\lambda(t_0)$, are given by $\phi_p(t)$ and $\lambda_p(t)$, and these are the quantities that are plotted as the position tracks for each station. These amplified position tracks (Fig. 3) directly show the position history of each GNSS station and allow for the visual estimation of both linear velocity trends and deviations away from linear trends. Additionally, we encode time into the visual representation of the position track visualization by coloring each track with a smooth gradation from a starting color (indicating t_0) through a smooth variation to an ending color representing the final time in the position track. A disadvantage to the simple track amplification

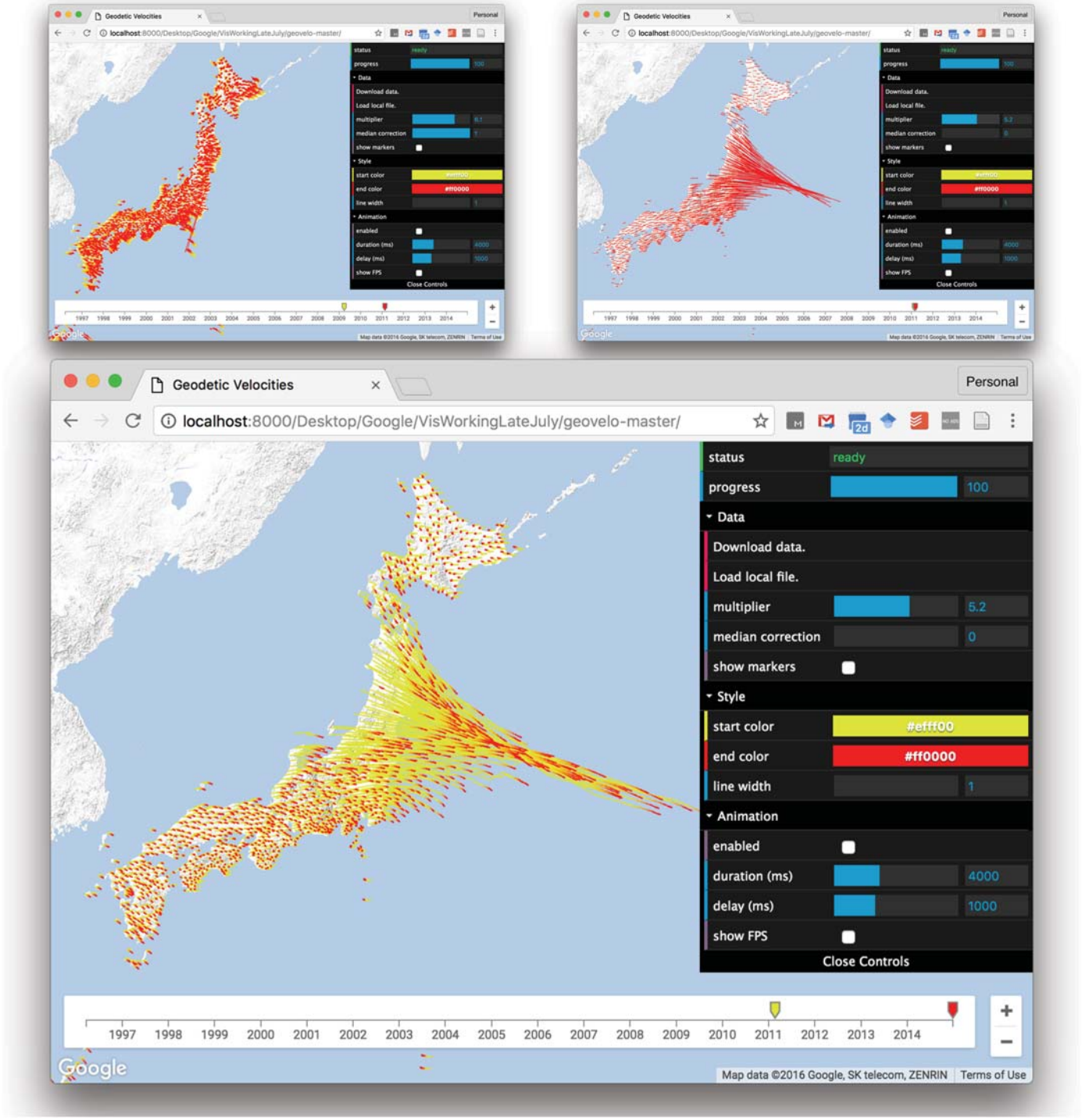

▲ **Figure 3.** Three static examples of track visualization GEONET GNSS position time series from Japan (e.g., Sagiya, 2004). Daily position time-series evolution are shown for each GNSS station as connected line segments colored yellow at the beginning of the observational epoch and grading to red as time advances. Background gray-scale shaded relief is derived from the Google Maps terrain layer database. The timeline along the bottom of the screenshots shows the complete time span of the data as well as the interval currently being displayed (February 1998 to November 2009). Time intervals can be dynamically localized or expanded using the epoch selection tool at the bottom. The upper-left panel shows nominally interseismic track movement toward Asia in the two years prior to the 2011 Tohoku-Oki earthquake. The upper-right panel shows the coseismic displacements on the day of the Tohoku-Oki earthquake characterized by trenchward motion toward the event epicenter. Across central and northern Honshu, this trend continues due to postseismic deformation in the years following the mainshock (lower panel).

method described here is that it does not adequately track across nonmonotonic variations in longitude and latitude (i.e., poles, prime meridian).

INTERACTING WITH TIME-SERIES POSITION TRACKS

The JavaScript application developed for this visualization (see Data and Resources) shows GNSS position time-series tracks on top of gray-scale shaded relief from the Google Maps terrain layer database to provide tectonic and geographic context. The GNSS position time-series data are loaded from a javascript object notation (JSON) file formatted as:

```
[
    {
      "name": "000841",
      "start": 985928400,
      "lon": [139.06990407, 139.069904, 139.06990413, ...],
      "lat": [34.949757897, 34.949757882, 34.949757941, ...]
    },{
      "name": "000842",
      "start": 982818000,
      "lon": [...],
      "lat": [...]
    },{
    ...
    {
      "name": "99R004",
      "start": 1364875200,
      "lon": [...],
      "lat": [...]
    },{
      "name": "99R006",
      "start": 1364875200,
      "lon": [...],
      "lat": [...]
    }
]
```

in which `name` is a string specifying the name of the GNSS station (should be unique), `start` is an integer specifying the Unix timestamp of the first GNSS reading, and `lon` and `lat` are arrays of floating point numbers giving the station longitude and latitude positions at daily intervals. The longitude and latitude arrays must be of the same length for each station, but they may be distinct at different stations. Zero longitude and latitude are treated as special values indicating missing data. A JSON file with these data can be loaded by clicking on the "Load local file" button. For an example of data sets derived from the GEONET array in Japan and PBO array in the United States, see Data and Resources.

In addition to the standard Google Maps navigation features, the interactive nature of this GNSS position track visualization is characterized by four main features: (1) temporal windowing, (2) control of amplification scale, (3) median position corrections, and (4) color encoding of time. The temporal window of the displayed tracks is not fixed at the first and last date of the available data. Instead, it can be specified and controlled by a time line at the bottom of the visualization (Fig. 3). This enables the track visualization to be temporally localized on an event of interest (e.g., the 2011 Tohoku-Oki earthquake). At smaller time intervals, GNSS tracks may appear relatively short in the absence of significant coseismic activity or too long as a result of large coseismic displacements. The track scaling magnitude α can be adjusted by dragging the "multiplier" slider. Larger and smaller multiplier values produce longer and shorter track lengths, respectively. Position estimates may be modified by a "median correction," ranging from 0 to 1, in which 0 indicates no median correction. This adjustment to the time series subtracts the median position from each component time series on a station-by-station basis. In some cases, this may lead to less noisy visualizations of interseismic tracks. Selectable colors ("start color", "end color") can be used to encode the relative time along a GNSS track. For example, in Figure 3, yellow indicates the start of selected epoch, and the color grades to red which characterizes the end of the selected epoch. Additionally, the GNSS position tracks may be animated by selecting the "enable" check box under the "Animation" tab. This feature will continually draw day-by-day track updates, returning to the starting date once the end date has been reached.

SUMMARY

We described a web-based application for analyzing time-dependent GNSS position time series in their geographic context that provides a way to simultaneously visualize the temporal and spatial evolution of these complex fields. As these data sets continue to grow ever larger, from tens to thousands of stations, there is an increasing need to be able to interactively interrogate these data to understand the spatial relationships between deformation across the entire earthquake cycle and to enable the discovery of new types of deformation at the Earth's surface.

DATA AND RESOURCES

An overview of the application and example data sets from Japan and the western United States can be downloaded from http://earthquake.rc.fas.harvard.edu (last accessed October 2016). The JavaScript application and example data sets can be downloaded from https://github.com/google/geovelo (last accessed October 2016). A python script to convert Plate Boundary Observatory style .pos time series to .json format can be obtained from https://github.com/brendanjmeade/PosToJson (last accessed October 2016). The data and sources cited in the text can be found in the websites: http://www.unavco.org/software/visualization/GPS-Velocity-Viewer/GPS-Velocity-Viewer.html (last accessed October 2016); http://www.unavco.org/projects/major-projects/pbo/pbo.html (last accessed October 2016); http://www.grapenthin.org/notes/2011_03_11-tohoku-oki/ (last accessed October 2016); http://geodesygina.com/BreathingEarth/index.html (last accessed October 2016);

http://sideshow.jpl.nasa.gov/post/series.html (last accessed October 2016). The MATLAB-based TSView tool can be found in http://www-gpsg.mit.edu/~tah/GGMatlab/ (last accessed October 2016). The JavaScript application used in this article can be found in https://geovelo.googlesource.com/geovelo/ (last accessed October 2016).

ACKNOWLEDGMENTS

We thank Zhigang Peng and two anonymous reviewers for offering comments on this article.

REFERENCES

Barbot, S., N. Lapusta, and J.-P. Avouac (2012). Under the hood of the earthquake machine: Toward predictive modeling of the seismic cycle, *Science* **336,** 707–710, doi: 10.1126/science.1218796.

Dragert, H., K. Wang, and T. S. James (2001). A silent slip event on the deeper Cascadia subduction interface, *Science* **292,** 1525–1528, doi: 10.1126/science.1060152.

Ergintav, S., S. McClusky, E. Hearn, R. Reilinger, C. Cakmak, T. Herring, H. Ozener, O. Lenk, and E. Tari (2009). Seven years of postseismic deformation following the 1999, $M = 7.4$ and $M = 7.2$, Izmit-Duzce, Turkey earthquake sequence, *J. Geophys. Res.* **114,** no. B07403, doi: 10.1029/2008JB006021.

Feigl, K. L., D. C. Agnew, Y. Bock, D. Dong, A. Donnellan, B. H. Hager, T. A. Herring, D. D. Jackson, T. H. Jordan, R. W. King, *et al.* (1993). Space geodetic measurement of crustal deformation in central and southern California, 1984–1992, *J. Geophys. Res.* **98,** 21,677–21,712, doi: 10.1029/93JB02405.

Feigl, K. L., R. W. King, and T. H. Jordan (1990). Geodetic measurement of tectonic deformation in the Santa Maria fold and thrust belt, California, *J. Geophys. Res.* **95,** 2679–2699, doi: 10.1029/JB095iB03p02679.

Graham, S. E., C. DeMets, E. Cabral-Cano, V. Kostoglodov, A. Walpersdorf, N. Cotte, M. Brudzinski, R. McCaffrey, and L. Salazar-Tlaczani (2014). GPS constraints on the 2011–2012 Oaxaca slow slip event that preceded the 2012 March 20 Ometepec earthquake, southern Mexico, *Geophys. J. Int.* **197,** 1593–1607, doi: 10.1093/gji/ggu019.

Grapenthin, R., and J. T. Freymueller (2011). The dynamics of a seismic wave field: Animation and analysis of kinematic GPS data recorded during the 2011 Tohoku-oki earthquake, Japan, *Geophys. Res. Lett.* **38,** L18308, doi: 10.1029/2011GL048405.

Hager, B. H., R. W. King, and M. H. Murray (1991). Measurement of crustal deformation using the Global Positioning System, *Annu. Rev. Earth Planet. Sci.* **19,** 351–382, doi: 10.1146/annurev.ea.19.050191.002031.

Herring, T. A. (2003). MATLAB tools for viewing GPS velocities and time series, *GPS Solut.* **7,** 194–199, doi: 10.1007/s10291-003-0068-0.

Kreemer, C., G. Blewitt, and E. C. Klein (2014). A geodetic plate motion and global strain rate model, *Geochem. Geophys. Geosys.* **15,** 3849–3889, doi: 10.1002/2014GC005407.

Loveless, J. P., and B. J. Meade (2010). Geodetic imaging of plate motions, slip rates, and partitioning of deformation in Japan, *J. Geophys. Res.* **115,** no. B02410, doi: 10.1029/2008JB006248.

Loveless, J. P., and B. J. Meade (2016). Two decades of spatiotemporal variations in subduction zone coupling offshore Japan, *Earth Planet. Sci. Lett.* **436,** 19–30, doi: 10.1016/j.epsl.2015.12.033.

Mavrommatis, A. P., P. Segall, and K. M. Johnson (2014). A decadal-scale deformation transient prior to the 2011 M_w 9.0 Tohoku-oki earthquake, *Geophys. Res. Lett.* **41,** 4486–4494, doi: 10.1002/2014GL060139.

Meade, B. J., and J. P. Loveless (2009). Predicting the geodetic signature of $M_w \geq 8$ slow slip events, *Geophys. Res. Lett.* **36,** L01306, doi: 10.1029/2008GL036364.

Nishimura, T., T. Hirasawa, S. Miyazaki, T. Sagiya, T. Tada, S. Miura, and K. Tanaka (2004). Temporal change of interplate coupling in northeastern Japan during 1995–2002 estimated from continuous GPS observations, *Geophys. J. Int.* **157,** 901–916, doi: 10.1111/j.1365-246X.2004.02159.x.

Radiguet, M., F. Cotton, M. Vergnolle, M. Campillo, B. Valette, V. Kostoglodov, and N. Cotte (2011). Spatial and temporal evolution of a long term slow slip event: The 2006 Guerrero slow slip event, *Geophys. J. Int.* **184,** 816–828, doi: 10.1111/j.1365-246X.2010.04866.x.

Sagiya, T. (2004). A decade of GEONET: 1994–2003—The continuous GPS observation in Japan and its impact on earthquake studies, *Earth Planets Space* **56,** xxix–xli, doi: 10.1186/BF03353077.

Savage, J. C., and J. L. Svarc (1997). Postseismic deformation associated with the 1992 $M_w = 7.3$ Landers earthquake, southern California, *J. Geophys. Res.* **102,** 7565–7577, doi: 10.1029/97JB00210.

Sella, G. F., T. H. Dixon, and A. Mao (2002). REVEL: A model for recent plate velocities from space geodesy, *J. Geophys. Res.* **107,** doi: 10.1029/2000JB000033.

Shen, Z.-K., X. Ge, D. D. Jackson, D. Potter, M. Cline, and L.-Y. Sung (1996). Northridge earthquake rupture models based on the Global Positioning System measurements, *Bull. Seismol. Soc. Am.* **86,** 37–48.

Simons, M., S. E. Minson, A. Sladen, F. Ortega, J. Jiang, S. E. Owen, L. Meng, J.-P. Ampuero, S. Wei, R. Chu, *et al.* (2011). The 2011 magnitude 9.0 Tohoku-oki earthquake: Mosaicking the megathrust from seconds to centuries, *Science* **332,** 1421–1425, doi: 10.1126/science.1206731.

Wang, Q., Q. Xuejun, L. Qigui, J. Freymueller, Y. Shaomin, X. Caijun, Y. Yonglin, Y. Xinzhao, T. Kai, and C. Gang (2011). Rupture of deep faults in the 2008 Wenchuan earthquake and uplift of the Longmen Shan, *Nat. Geosci.* **4,** 634–640, doi: 10.1038/ngeo1210.

Wernicke, B., and J. L. Davis (2010). Detecting large-scale intracontinental slow-slip events (SSEs) using geodograms, *Seismol. Res. Lett.* **81,** 694–698, doi: 10.1785/gssrl.81.5.694.

Brendan J. Meade
Department of Earth and Planetary Sciences
Harvard University
Cambridge, Massachusetts 02138 U.S.A.
meade@fas.harvard.edu

William T. Freeman[1]
Department of Electrical Engineering and Computer Science
Massachusetts Institute of Technology
Cambridge, Massachusetts 02139 U.S.A.

James Wilson
Fernanda Viegas
Martin Wattenberg
Google
Cambridge, Massachusetts 02139 U.S.A.

Published Online 23 November 2016

[1] Also at Google, Cambridge, Massachusetts 02139 U.S.A.